Imaging finding of multiple myeloma presenting as soft-tissue disease mimicking extrapleural space tumors: A case report

Hee Kang [ORCID]

Abstract

Extramedullary involvement of multiple myeloma is an uncommon and aggressive condition characterized by proliferation of monoclonal plasma cells located outside the bone marrow. This report describes the imaging findings of a patient who presented with continuous soft-tissue disease on the ribs, suspected as extrapleural space tumors on chest CT. The patient was diagnosed with multiple myeloma through surgical biopsy of the tumor and bone marrow.

Introduction

Multiple myeloma (MM) constitutes up to 1% of all cancers and accounts for 15% of hematological malignancies. This disease is characterized by proliferation of malignant clonal plasma cells and production of a large number of monoclonal immunoglobulins. MM is primarily confined to the bone marrow and skeleton. Clinical manifestations are related to organ damage and/or tissue impairment, presenting as the so-called CRAB symptoms (hypercalcemia, renal insufficiency, anemia, and/or bone lesion). However, in some instances, patients may develop soft-tissue extramedullary plasmacytomas, which could manifest as more prominent clinical features.[1,2] Although rare, thoracic involvement has been reported in MM patients, presenting as varied thoracic manifestations such as lung mass, diffuse interstitial infiltration, multiple pulmonary nodules, lymphadenopathy, mediastinal mass, tracheobronchial infiltration, and nodular pleural thickening accompanied by pleural effusion.[3,4]

Herein, we present the multimodality imaging findings of a patient with MM, manifested as continuous soft-tissue disease on the ribs without cortical destruction, mimicking extrapleural space tumors of the thorax.

Case presentation

A 63-year-old man complained of mild dyspnea and fatigue for several months. He had been on medication for chronic obstructive pulmonary disease. On physical examination, dullness with decreased breath sound was noted over the left hemithorax. His maximum temperature was 37.5°C.

Chest radiography revealed bilateral pleural effusions, with more on the left side. Additionally, there were somewhat increased bronchovascular bundle markings and

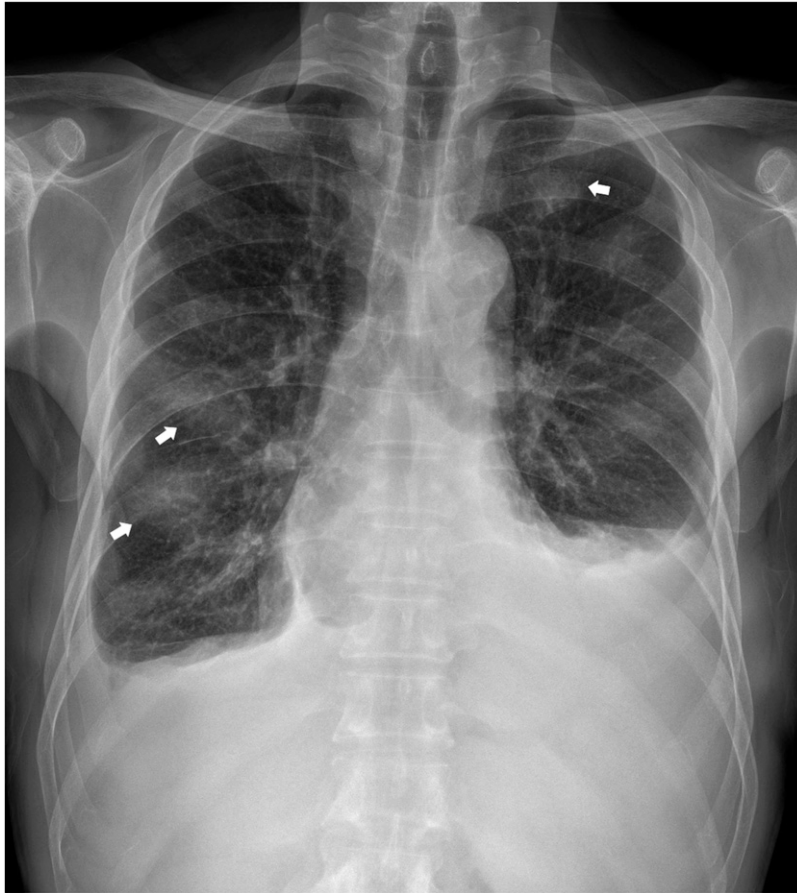Department of Radiology, Kosin University Gospel Hospital, Kosin University College of Medicine, Busan, Korea

Corresponding author:
Hee Kang, Department of Radiology, Kosin University Gospel Hospital, Kosin University College of Medicine, 262 Gamcheon-ro, Seo-gu, Busan 49267, South Korea.
Email: kanghi81@gmail.com

Figure 1. Chest radiography reveals bilateral pleural effusions, with more on the left side. Additionally, there were somewhat increased bronchovascular bundle markings and ill-defined patchy opacities (arrows) in both hemithoraces.

ill-defined patchy opacities in both hemithoraces (Figure 1). He underwent pleural fluid drainage, analysis of which revealed an elevated adenosine deaminase level of 59.7 U/L and a lymphocyte proportion of 72%.

Contrast-enhanced chest CT scan revealed multifocal extrapleural soft-tissue masses and residual pleural effusion in both hemithoraces. On the oblique axial reconstruction image, the lesions appeared as a continuous band-like soft tissue density with a smooth margin along each rib. On the coronal and sagittal images, the lesions were surrounding the inner surface of each rib. On the CT scans, normal trabeculae were observed with no evidence of cortical destruction of the ribs (Figure 2). Additionally, diffuse and mild bronchial wall and interlobular septal thickening with bilateral pleural effusion suggestive of pulmonary edema was observed on the lung window images (not shown here).

Whole body diffuse-weighted imaging (DWI) exhibited diffusely increased signal intensity of the bone marrow of the visible skeleton, including spine, ribs, and pelvis. On the apparent diffusion coefficient (ADC) map, the signal intensity of the lesion was low but was higher than that of apparently normal bone marrow. Postcontrast coronal T1-weighted MRI with fat suppression revealed diffuse enhancement of the bone marrow of each rib, accompanied by extraosseous soft tissue disease (Figure 3). The soft tissue lesions exhibited high-signal intensity on DWI and low-signal intensity on ADC map (not shown here). Maximum intensity projection of fluorodeoxyglucose-positron emission tomography (FDG-PET) showed hypermetabolic activity in multiple bones and diffuse lesions with mild hypermetabolism along both ribs (Figure 4). The patient underwent video-assisted thoracoscopic surgery (VATS) for a biopsy of the soft-tissue disease. Thoracoscopy revealed multiple masses along each rib, covered by parietal pleura (Figure 5). Microscopic finding of the surgical specimen was diffuse plasma cell proliferation composed of a mixture of mature and immature plasma cells and plasmacytic cells. Immunohistochemical staining demonstrated diffuse positive staining for CD138 and lambda chain restriction (Figure 6).

The patient underwent a bone marrow biopsy, which revealed 34% plasma cells with partial nuclear atypia such as prominent nucleoli. Additionally, there was evidence of lambda light chain restriction and positive expression of
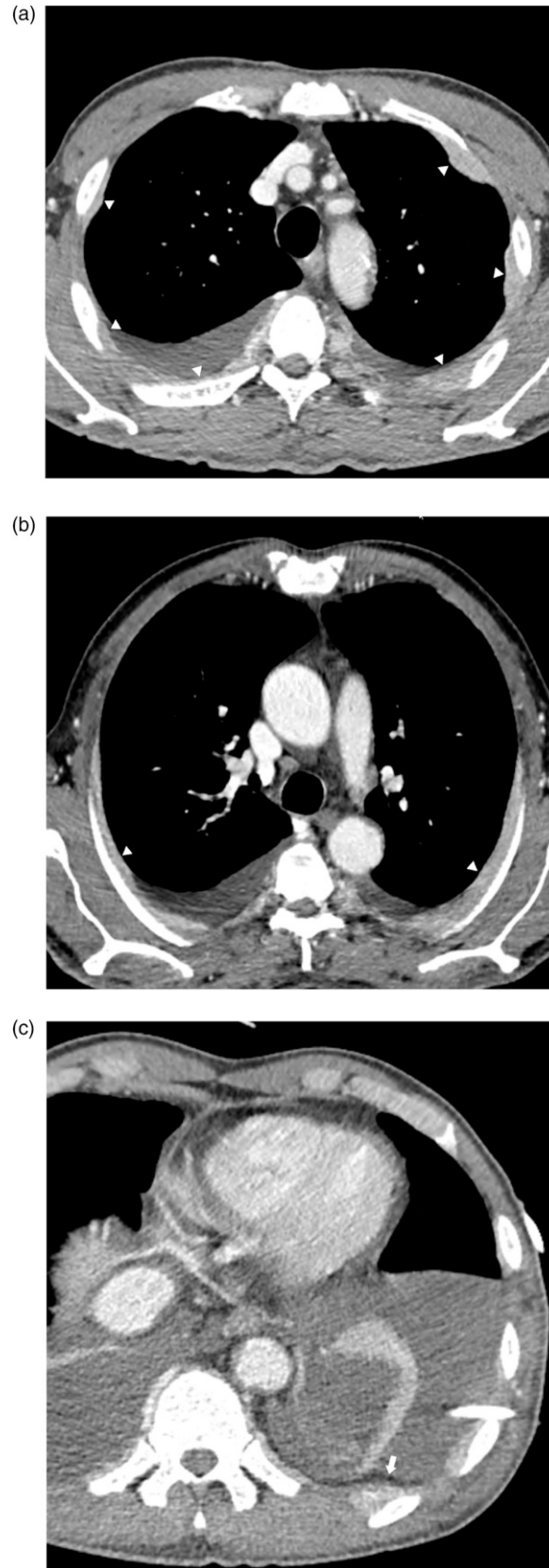
Figure 2. (a) Axial view contrast-enhanced chest CT scan reveals multifocal pleural nodular lesions (arrowheads) and residual pleural effusion in both hemithoraces. (b) On the oblique axial reconstruction image, the lesions appear as a continuous band-like soft tissue density with a smooth margin (arrowheads) along each rib. (c) At the level of the diaphragm, the lesions are located outside of the extrapleural fat (arrow). (d) and (e) On the coronal and sagittal images, the lesions are surrounding the inner surface of each rib (arrowheads).
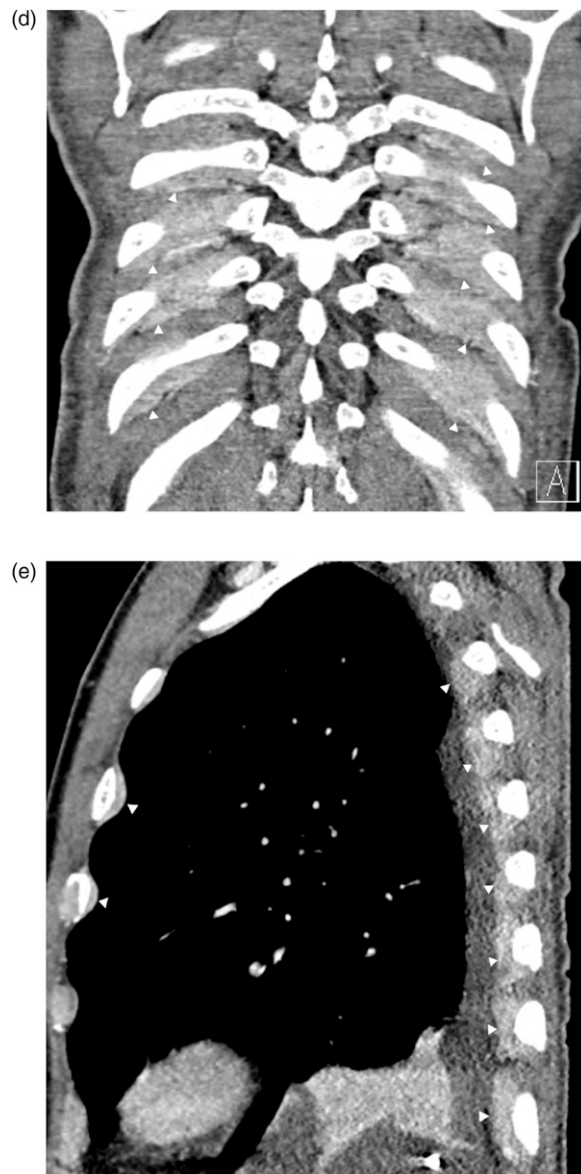
Figure 2. Continued.

CD138. Bence–Jones protein was also detected in the urinalysis, leading to the diagnosis of MM. The patient commenced bortezomib–lenalidomide–dexamethasone triple therapy.

Discussion

MM is the most frequent cancer to involve the skeleton, with 80%–90% of patients developing bone lesions. Myeloma bone lesions are purely osteolytic and are associated with bone pain, pathologic fractures, hypercalcemia, spinal cord compression, and increased mortality.[5] Although plasma cell proliferation is confined to the bone marrow in

most patients with MM, a subset of patients develops soft-tissue involvement, with clonal plasma cells found outside the bone marrow. Extramedullary disease of MM often represents an aggressive form characterized by the ability of a clone and subclone to thrive and grow independent of the bone marrow microenvironment.[6]

A previous expert consensus review has endorsed the definition and distinction of soft-tissue involvement in MM: (a) paraskeletal involvement with tumor masses arising from skeletal lesions and (b) extramedullary involvement with hematogenous spread involving only soft tissue. The mechanism resulting in soft tissue plasmacytomas is direct growth from skeletal tumors by disrupting the cortical bone,
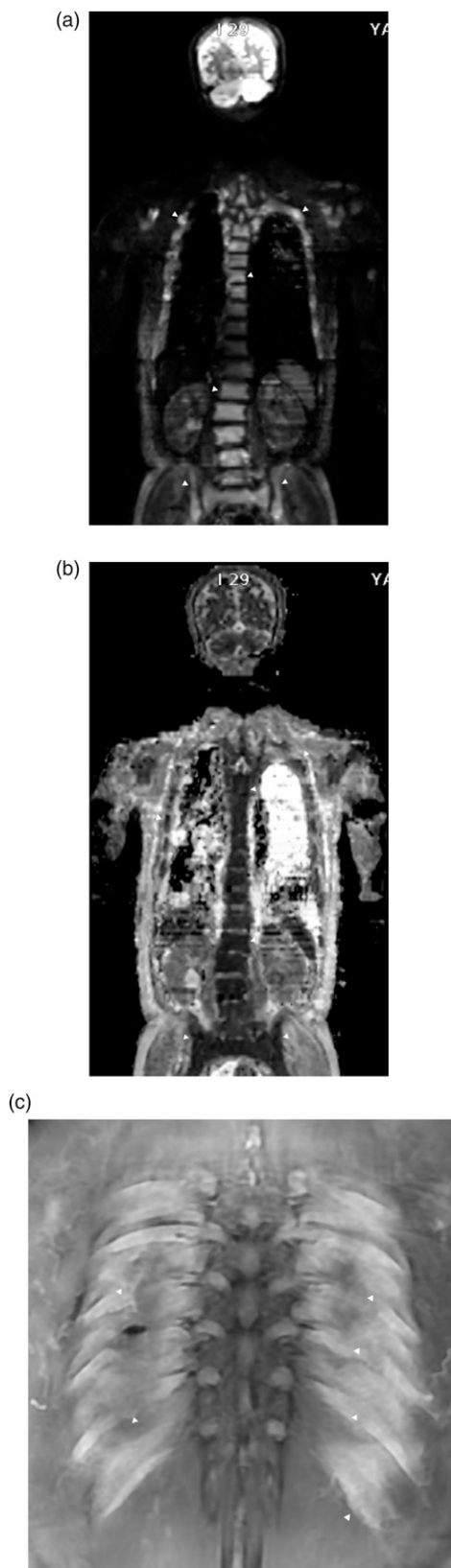
Figure 3. (a) Whole body diffuse-weighted imaging (DWI) (b value = 800 s/mm^2) exhibits diffusely increased signal intensity of the bone marrow of the visible skeleton, including spine, ribs, and pelvis (arrowheads). (b) On the apparent diffusion coefficient (ADC) map, the signal intensity of the lesion is low but is higher than that of apparently normal bone marrow (arrowheads). (c) Postcontrast coronal T1-weighted MRI with fat suppression reveals diffuse enhancement of the bone marrow of each rib, accompanied by extraosseous soft tissue disease (arrowheads).

Figure 4. Maximum intensity projection of fluorodeoxyglucose-positron emission tomography (FDG-PET) shows hypermetabolic activity in multiple bones (arrowheads) and diffuse lesions with mild hypermetabolism along both ribs (asterisks).
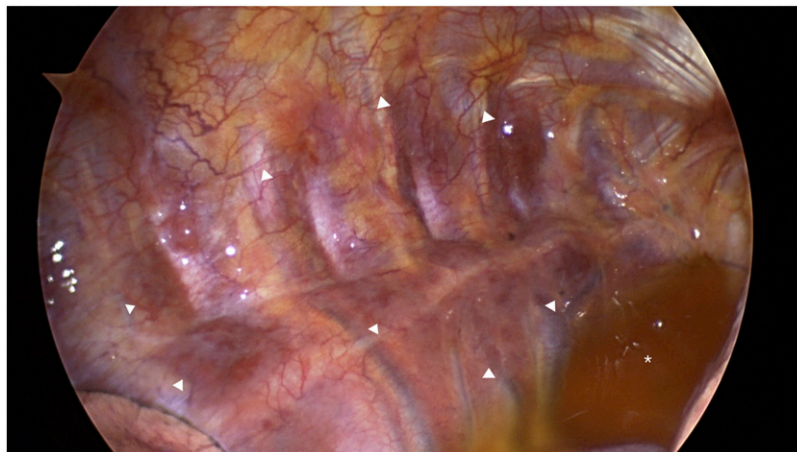
Figure 5. Thoracoscopy reveals multiple masses (arrowheads) along each rib, covered by parietal pleura. Focal pleural effusion (asterisk) is seen.

while the remaining tumors result from hematogenous spread without contact with bony structures.[2]

In a prior meta-analysis, the overall incidence of soft-tissue plasmacytomas was 18.2%, with paraskeletal involvement in 14.5% and extramedullary involvement in 3.7% at new diagnosis.[7] The reported incidence rates vary considerably, which may be due to variations in diagnostic approaches among studies. This variability might also stem from heterogeneous populations including patients with new diagnoses of MM and relapsed MM. Furthermore, the lack of a clear distinction between bone-related plasmacytomas and exclusive extramedullary involvement likely contributes to this variability.

In the current case, chest CT did not reveal adjacent cortical destruction or definite osteolytic lesions, leading to the initial diagnosis of an extrapleural space tumor of the thorax. Subsequent MRI and PET-CT scans confirmed systemic diffuse bone marrow lesions, and a diagnosis of MM with thoracic paraskeletal involvement was established through VATS biopsy and bone marrow biopsy.

CT primarily helps to detect the destructive effects of myeloma disease on trabecular and cortical bone rather than disease within the bone marrow. If myeloma occupies the marrow spaces of long bones where it contrasts fatty bone marrow, it can be depicted on CT. However, in trabecular bones such as vertebral bodies, myeloma infiltrates are difficult to assess due to the trabeculae themselves or other concurrent degenerative changes or osteoporosis, especially in the population at risk.[8]

Whole-body MRI as currently used includes DW MRI sequences that are sensitive to cellular density and viability.[8] The excellent soft-tissue contrast of MRI allows direct imaging of the bone marrow, providing high sensitivity for detection of focal myeloma disease. Even before bone destruction occurs in early-stage MM patients, MRI can detect bone marrow lesions.[9–11] DWI MRI produces images in which the contrast between tissues is based on differences in the motion of water at a cellular level. Choice of diffusion weighting (b value) influences which compartments are assessed.[9] Imaging with more than one b-value enables automated calculation of an ADC for each pixel in the image, and a quantitative map can be produced. Tumors that consist of tightly packed cells exhibit areas of restricted diffusion, appearing as regions with high signal on source diffusion image and low-signal intensity on ADC.[12] ADC has a complex function in tissue microarchitecture and is sensitively influenced by several tissue components. The inverse correlation between the cell density of soft tissues and ADC has been widely documented.[13–16] However, cellularity is not the sole factor influencing ADC. Other factors, such as cellular architecture, cell size, and size variability within tissue; viscosity of cytoplasm; bulk flow in capillaries; and active transport, have been implicated as potential influencers of ADC values. Inclusion of DW MRI allows highly sensitive and quantitative evaluation of the soft tissue and bone marrow, and the relationship of ADC values with cell density facilitates response assessments, allowing evaluation not only of changes in lesion size but also treatment response in MM patients.[9]

PET-CT obtains information about cellular metabolic activity using radioactive substances; the most commonly used is fluorodeoxyglucose (FDG) containing 18F. The FDG uptake on PET-CT images signifies the metabolic activity of myeloma cells, reflecting active myeloma lesions. This modality not only evaluates bone lesions but also detects extramedullary lesions. PET-CT is acknowledged as the optimal standard diagnostic method for evaluating and monitoring treatment response in MM.[17,18]

In conclusion, soft-tissue disease in MM rarely manifests as continuous tumors on ribs without evident bone destruction in both thoraces, mimicking an extrapleural space tumor on CT. Comprehensive imaging modalities including
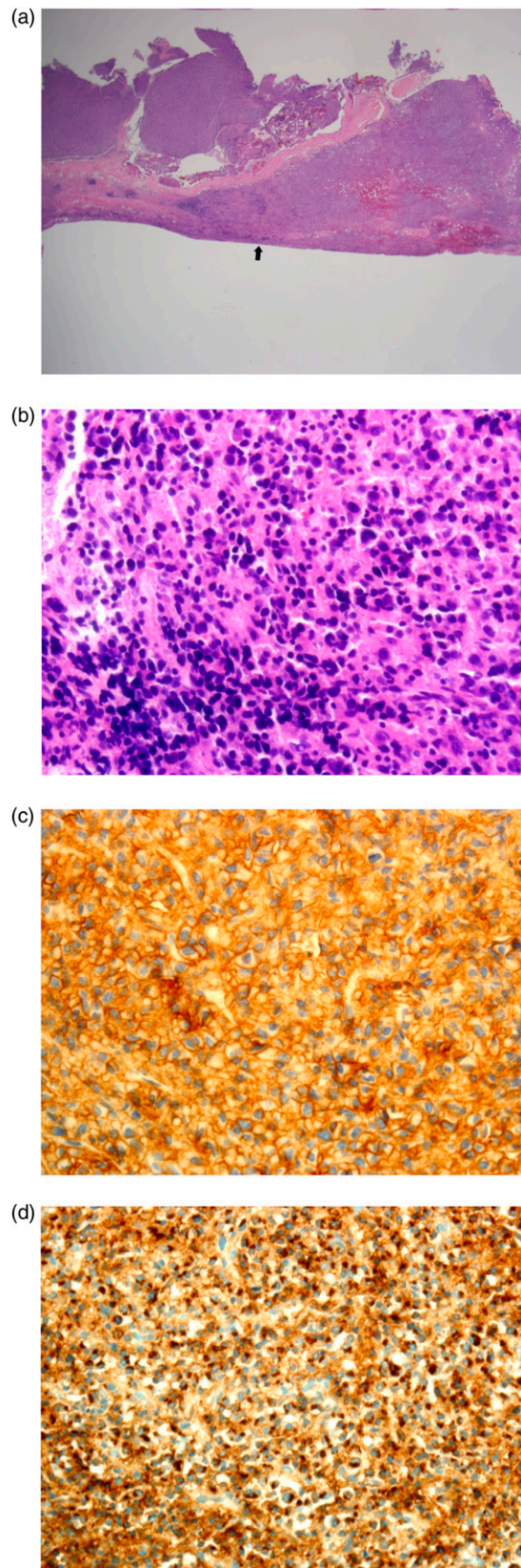
Figure 6. (a) Microscopy of the surgical specimen at low magnification (H&E stain, ×12.5) reveals a hypercellular, small, round cell tumor with a smooth margin along the pleural side (arrow). (b) At high-power magnification of ×400, diffuse plasma cell proliferation is observed, composed of a mixture of mature and immature plasma cells and plasmacytic cells. Immunohistochemical staining demonstrates diffuse positive staining for CD138 (c) and lambda chain restriction (d).

MRI and PET-CT play pivotal roles in the early detection and characterization of disease distribution in MM patients who do not present with definitive osteolytic lesions.

Declaration of conflicting interests

Funding

Ethical statement

Ethical approval

Institutional review board (IRB) approval was obtained for this report, and the need for informed consent was waived.

ORCID iD

Hee Kang ⬤ https://orcid.org/0000-0001-8065-5477

References

1. Blade J, Fernandez de Larrea C, Rosinol L, et al. Soft-tissue plasmacytomas in multiple myeloma: incidence, mechanisms of extramedullary spread, and treatment approach. J Clin Oncol 2011; 29: 3805–3812.

2. Rosinol L, Beksac M, Zamagni E, et al. Expert review on soft-tissue plasmacytomas in multiple myeloma: definition, disease assessment and treatment considerations. Br J Haematol 2021; 194: 496–507.

3. Saha R, Bhattacharya A, Deb J, et al. Multiple myeloma presenting as thoracic plasmacytoma–two rare cases. Egypt J Chest Dis Tuberc 2014; 63: 267–271.

4. Yeoh KW, Thitsar SM, Master Z, et al. Pleural plasmacytomas - the role of radiotherapy. Br J Haematol 2020; 190: e160–e162.

5. Silbermann R, Roodman GD. Myeloma bone disease: pathophysiology and management. J Bone Oncol 2013; 2: 59–69.

6. Blade J, Beksac M, Caers J, et al. Extramedullary disease in multiple myeloma: a systematic literature review. Blood Cancer J 2022; 12: 45.

7. Gagelmann N, Eikema DJ, Iacobelli S, et al. Impact of extramedullary disease in patients with newly diagnosed multiple myeloma undergoing autologous stem cell transplantation: a study from the Chronic Malignancies Working Party of the EBMT. Haematologica 2018; 103: 890–897.

8. Messiou C, Hillengass J, Delorme S, et al. Guidelines for acquisition, interpretation, and reporting of whole-body MRI in myeloma: myeloma response assessment and diagnosis system (MY-RADS). Radiology 2019; 291: 5–13.

9. Messiou C, Kaiser M. Whole body diffusion weighted MRI-- a new view of myeloma. Br J Haematol 2015; 171: 29–37.

10. Moulopoulos LA, Dimopoulos MA, Weber D, et al. Magnetic resonance imaging in the staging of solitary plasmacytoma of bone. J Clin Oncol 1993; 11: 1311–1315.

11. Son AY, Chung HW. [Imaging for multiple myeloma according to the recent international myeloma working group guidelines: analysis of image acquisition techniques and response evaluation in whole-body MRI according to MY-RADS]. J Korean Soc Radiol 2023; 84: 150–169.

12. Messiou C, deSouza NM. Metastasis imaging: current concepts and future challenges. Cancer Biomarkers 2010; 7: 171–172.

13. Sugahara T, Korogi Y, Kochi M, et al. Usefulness of diffusion-weighted MRI with echo-planar technique in the evaluation of cellularity in gliomas. J Magn Reson Imag 1999; 9: 53–60.

14. Lyng H, Haraldseth O, Rofstad EK. Measurement of cell density and necrotic fraction in human melanoma xenografts by diffusion weighted magnetic resonance imaging. Magn Reson Med 2000; 43: 828–836.

15. Tamai K, Koyama T, Saga T, et al. The utility of diffusion-weighted MR imaging for differentiating uterine sarcomas from benign leiomyomas. Eur Radiol 2008; 18: 723–730.

16. Ormond Filho AG, Carneiro BC, Pastore D, et al. Whole-body imaging of multiple myeloma: diagnostic criteria. Radiographics 2019; 39: 1077–1097.

17. Lee K, Kim KW, Ko Y, et al. Comprehensive updates in the role of imaging for multiple myeloma management based on recent international guidelines. Korean J Radiol 2021; 22: 1497–1513.

18. Cavo M, Terpos E, Nanni C, et al. Role of (18)F-FDG PET/CT in the diagnosis and management of multiple myeloma and other plasma cell disorders: a consensus statement by the International Myeloma Working Group. Lancet Oncol 2017; 18: e206–e217.